

# A RATE-DEPENDENT MULTI-SCALE CRACK MODEL FOR CONCRETE

AMIN KARAMNEJAD\*, VINH P. NGUYEN<sup>†</sup> AND LAMBERTUS J. SLUYS\*

\*Delft University of Technology, Faculty of Civil Engineering and Geosciences  
P.O. Box 5048, 2600 GA Delft, The Netherlands  
e-mails: A.Karamnejad@tudelft.nl, L.J.Sluys@tudelft.nl

<sup>†</sup> Ton Duc Thang University, Division of Computational Mechanics  
Hochiminh City, Vietnam  
e-mail: nvinhphu@gmail.com

**Key words:** Dynamic Loading, Computational Homogenization, Multi-scale Cohesive Law, Representative Volume Element (RVE)

**Abstract.** A multi-scale numerical approach for modeling cracking in heterogeneous quasi-brittle materials under dynamic loading is presented. In the model, a discontinuous crack model is used at macro-scale to simulate fracture and a gradient-enhanced damage model has been used at meso-scale to simulate diffuse damage. The traction-separation law for the cohesive zone model at macro-scale is obtained from the meso-scale information through the discontinuous computational homogenization method. The method is based on the so-called failure zone averaging scheme in which the averaging theorem is used over the active damaged zone of the meso-scale. Objectivity with respect to the local-scale sample size in the softening regime is obtained in this fashion. In order to evaluate the macroscopic traction at each integration point on the crack, at each time step of the macro model solution, a static boundary value problem is solved for the representative volume element (RVE) whose size is much smaller than the macro length-scale and the macroscopic wave-length. The effect of the crack opening rate on the macro cohesive law is taken into account by relating the material properties of the meso-scale model to the macro crack opening rate. The objectivity of the model response with respect to the representative volume element (RVE) size is demonstrated for wave propagation problems. The rate-dependent multi-scale model is then verified by comparison with a direct numerical simulation (DNS).

## 1 INTRODUCTION

Macroscopic behavior of concrete is determined by its heterogeneous microstructure. Initiation and propagation of the crack in concrete is controlled by its randomness and occurs at different length scales. Multi-scale approaches provide methodologies to obtain overall behavior of a heterogeneous material from its local scales. Computational homogenization is a multi-scale method in which the heterogeneous material is replaced by a homogeneous substitute with unknown macroscopic constitu-

tive behavior. Then, a representative volume element (RVE) is associated to each material point and the constitutive law is obtained by solving a boundary value problem for the RVE. A sample volume can be defined as RVE when homogenized properties do not change significantly with varying RVE size. An RVE can be defined in linear and hardening regimes but in the softening regime an RVE cannot be defined using standard computational homogenization scheme [1]. A discontinuous computational homogenization scheme is developed in [2] which

is objective with respect to the RVE size and is formulated based on a failure zone averaging method [3]. A continuous-discontinuous scheme which is a combination of standard homogenization scheme and discontinuous homogenization scheme is also given in [4]. In this scheme, the crack initiation is detected by localization analysis of local-scale model using limit point criterion while the crack direction is taken perpendicular to the direction of maximum principle macroscopic stress.

Multi-scale modeling of heterogeneous material under dynamic loading is studied by a number of researchers. For instance, wave dispersion effects are modeled in [5, 6] using a two-scale asymptotic expansion method. A multi-scale model for heterogeneous viscoelastic solids under dynamic loading is presented by Souza et. al. [7, 8]. In their model, the homogenized tangent and stress tensor depend on damage accumulated in the local-scale model.

In the present work, the discontinuous and continuous-discontinuous computational homogenization schemes given in [2, 4] are extended to model cracking in concrete under dynamic loading. In the modified continuous-discontinuous scheme, in addition to crack initiation, the direction of the macroscopic crack is also determined from a local-scale model. Rate effects are also added to the model by relating the material properties of the RVE to the rate of the macroscopic crack opening.

## 2 MULTI-SCALE MODEL

A standard computational homogenization scheme is valid until strain localization occurs in the material. After damage, the solution depends on the size of the local-scale and an RVE does not exist. In order to overcome this problem, a discontinuous homogenization scheme is developed which uses stress/strain averaging over the localization band (failure zone averaging method) instead of the whole domain. Alternatively, a continuous-discontinuous scheme combines standard and discontinuous homogenization schemes. In this method, the constitutive law of the macro-scale model is obtained

using the standard homogenization scheme in hardening regime. When a localization occurs in the RVE associated to a certain macro material point, a crack initiates at that point and the cohesive law for the crack is determined using the discontinuous homogenization scheme. In the present multi-scale model, dynamic problems in which the macro-scale wave length is significantly larger than the local-scale characteristic length, are considered. In such conditions, it is possible to neglect dynamics at the local-scale model. So, in the following multi-scale model, at macro-scale a dynamic problem is solved and at each time step, in order to calculate the homogenized properties, a quasi-static problem is solved for the local-scale model. The macrocrack is modeled as a strong discontinuity using XFEM [9] and a gradient-enhanced damage model [10] is used to model diffuse damage at the meso-scale.

### 2.1 Macro-scale model

Macro cracking is modeled using the XFEM. In the finite element model, the momentum equation can be written as:

$$\mathbf{M}\ddot{\mathbf{u}}_M = \mathbf{f}_M^{ext} - (\mathbf{f}_M^{bulk} + \mathbf{f}_M^{coh}) \quad (1)$$

where  $\ddot{\mathbf{u}}_M$  represents the macroscopic acceleration vector,  $\mathbf{M}$  is the mass matrix.  $\mathbf{f}_M^{ext}$  is the external force vector,  $\mathbf{f}_M^{bulk}$  and  $\mathbf{f}_M^{coh}$  represent the bulk force vector and the cohesive force vector, respectively and are given as:

$$\begin{aligned} \mathbf{f}_M^{bulk} &= \int_{\Omega_M} \mathbf{B}^T \boldsymbol{\sigma}_M d\Omega, \\ \mathbf{f}_M^{coh} &= \int_{\Gamma_M^d} \mathbf{N}^T \mathbf{t}_M d\Gamma \end{aligned} \quad (2)$$

in which  $\mathbf{t}_M$  is the macro-scale traction and  $\mathbf{N}$  and  $\mathbf{B}$  are the matrix of nodal shape functions and the matrix of derivatives of the shape functions, respectively. The bulk macro-stress can be computed as:

$$\boldsymbol{\sigma}_M = \mathbf{D}_M : \boldsymbol{\varepsilon}_M \quad (3)$$

The fourth-order tensor  $\mathbf{D}_M$  is the bulk homogenized tensor which can be computed using a standard homogenization technique. The macro

traction,  $\mathbf{t}_M$ , is obtained from the cohesive law via:

$$\dot{\mathbf{t}}_M = \mathbf{T}_M \cdot \dot{[\mathbf{u}]}_M \quad (4)$$

where  $[\mathbf{u}]_M$  is the displacement jump for the macro crack and  $\mathbf{T}_M$  is the macro cohesive tangent. At each time step, the displacement jump is obtained for each integration point on the crack and the corresponding macro traction,  $\mathbf{t}_M$ , and macro cohesive tangent,  $\mathbf{T}_M$ , are computed using the discontinuous homogenization scheme from the meso-scale model.

## 2.2 Meso-scale model

At meso-scale, failure is modeled using the implicit gradient-enhanced damage model [10]. The stress-strain relation is given as [11]:

$$\boldsymbol{\sigma}_m = (1 - \omega) \mathbf{D}_m : \boldsymbol{\varepsilon}_m \quad (5)$$

where  $\omega$  is the scalar damage variable ( $0 \leq \omega \leq 1$ ) and  $\mathbf{D}_m$  is a fourth-order tensor which contains the elastic moduli of meso-scale constituents. The damage evolution law is written as:

$$\omega = \begin{cases} 0 & \text{if } \kappa \leq \kappa_I \\ 1 - \frac{\kappa}{\kappa_I} [1 - \gamma + \gamma e^{-\beta(\kappa - \kappa_I)}] & \text{if } \kappa > \kappa_I \end{cases} \quad (6)$$

where  $\gamma$ ,  $\beta$  and  $\kappa_I$  denote residual stress, softening slope and damage threshold, respectively.  $\kappa$  is a scalar measure of the largest strain ever reached and is defined by loading function  $f$  as:

$$f = \bar{\varepsilon}_{eq} - \kappa \quad (7)$$

$f$  and  $\kappa$  satisfy the Kuhn-Tucker conditions:

$$f \leq 0, \quad \dot{\kappa} \geq 0, \quad f \dot{\kappa} = 0 \quad (8)$$

$\bar{\varepsilon}_{eq}$  is the nonlocal equivalent strain which is implicitly related to the local equivalent strain according to [10]:

$$\bar{\varepsilon}_{eq} - c \nabla^2 \bar{\varepsilon}_{eq} = \varepsilon_{eq} \quad (9)$$

In this equation,  $c$  is defined as  $c = \frac{1}{2} l_c^2$  and  $l_c$  represents the length scale at meso-scale. The local equivalent strain [12] is defined as:

$$\varepsilon_{eq} = \sqrt{\langle \varepsilon_1 \rangle^2 + \langle \varepsilon_2 \rangle^2} \quad (10)$$

where  $\varepsilon_i$  are the principle strains and  $\langle x \rangle$  refers to the positive part of  $x$ .

The discrete system of equations for meso-scale model (RVE) at time step  $t$  and iteration  $i$  in the macro-scale problem solution procedure can be written as:

$${}^{(t,i)} \mathbf{f}_m^{ext} = {}^{(t,i)} \mathbf{f}_m^{int} \quad (11)$$

where  ${}^{(t,i)} \mathbf{f}_m^{int}$  and  ${}^{(t,i)} \mathbf{f}_m^{ext}$  are the internal force vector and the external force vector for the meso-scale problem (at time step  $t$  and iteration  $i$  of the macro-scale problem solution), respectively. The external force vector for the meso-scale model is a function of the macroscopic displacement jump,  ${}^{(i,t)} [\mathbf{u}]_M$ . By solving equation (11) one can find the macro traction,  $\mathbf{t}_M$ , and macro cohesive tangent,  $\mathbf{T}_M$ , at time step  $t$  and iteration  $i$  for each integration point on the crack.

## 2.3 Homogenization schemes

Figure 1 shows the homogenization schemes that are used in the model in hardening and softening regimes. Before damage occurs in the material point, using standard computational homogenization scheme, the macro strain  $\boldsymbol{\varepsilon}_M$  can be transformed on the RVE boundary as (for periodic boundary condition) [13]:

$$\mathbf{u}_i = \mathbf{H}_i^T \boldsymbol{\varepsilon}_M \quad i = 1, 2, 4 \quad (12)$$

in which  $\mathbf{u}_i$  is the displacement of the RVE's three controlling nodes (figure 2) and  $\mathbf{H}_i$  is:

$$\mathbf{H}_i = \begin{bmatrix} x_i & 0 \\ 0 & y_i \\ \frac{y_i}{2} & \frac{x_i}{2} \end{bmatrix} \quad (13)$$

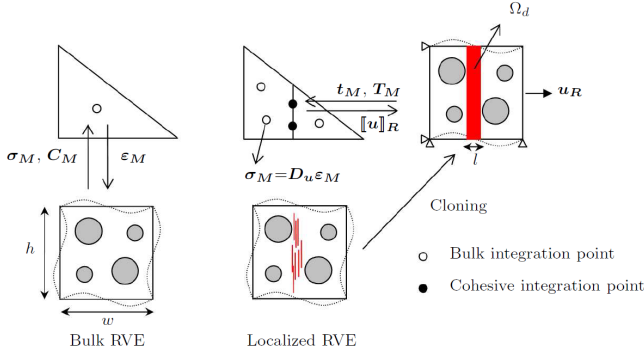


Figure 1: Computational homogenization scheme.

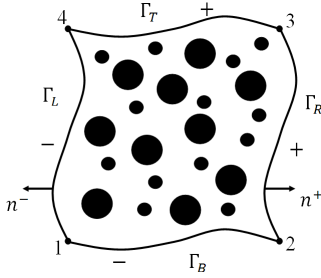


Figure 2: Periodic representative volume element.

From the definition of macroscopic stress as being the volume average of meso-scale stress, one can obtain:

$$\sigma_M = \frac{1}{|\Omega_m|} [H_1 \ H_2 \ H_4] \begin{bmatrix} f_1 \\ f_2 \\ f_4 \end{bmatrix} \quad (14)$$

where  $f_i$  is the force vector at controlling nodes. Furthermore, having the linear system of equations at the converged state for an RVE as  $K_{ii}\delta u_{ii} = \delta f_{ii}$ , the tangent moduli,  $C_M$ , can be derived as:

$$C_M = [H_1 \ H_2 \ H_4] (K_{bb} - K_{ba}K_{aa}^{-1}K_{ab}) \begin{bmatrix} H_1 \\ H_2 \\ H_4 \end{bmatrix} \quad (15)$$

in which subscript  $b$  denotes controlling nodes (three corner nodes) degrees of freedom and subscript  $a$  represents the other nodes' DOFs.

The macro-scale mass density can be related to the meso-scale mass density as [7]:

$$\rho_M = \frac{1}{|\Omega_m|} \int_{\Omega_m} \rho_m d\Omega \quad (16)$$

When localization is detected in the RVE associated to a certain integration point (at macro-scale model), a macrocrack is inserted in that point. In the cracked element (figure 1), the bulk integration points are disconnected from the meso-scale model. In the discontinuous homogenization scheme the bulk material properties are already known from pre-calculation using standard homogenization and in the continuous-discontinuous scheme, the macro stress can be obtained as:

$$\sigma_M = D_{un} \varepsilon_M \quad (17)$$

where  $D_{un}$  is a secant unloading matrix which can be computed by unloading the localized RVE and computing the homogenized tangent from equation 15. To each integration point on the crack surface, an RVE with boundary conditions shown in figure 1 is allocated. The macro-meso transition equation is given as:

$$u_R(u_m) = (w - l(u_m)) C t_M + [[u]]_M + u_{dam}^0 \quad (18)$$

where  $u_R$  is the total displacement at the right edge of the RVE. The first term in the RHS represents the linear displacement and  $u_{dam}^0$  is the compatibility displacement.  $w$  and  $l$  denote the width of the RVE and the averaged width of the localization band, respectively (figure 1). Matrix  $C$  is obtained as:

$$C = \Delta^T D^{-1} \Delta, \quad \Delta = \begin{bmatrix} 1 & 0 \\ 0 & 0 \\ 0 & 1 \end{bmatrix} \quad (19)$$

In a discontinuous homogenization scheme,  $D$  is equal to the homogenized tensor  $D_M$  while in a continuous-discontinuous scheme  $D$  can be computed using the cloning operation as follows: when localization is detected in the RVE associated to the bulk integration point, the average stress,  $\sigma_M^{loc}$ , is calculated from equation 14. The traction can be obtained using

$t_M^{loc} = \sigma_M^{loc} \cdot \mathbf{n}$ , where  $\mathbf{n}$  is the normal vector of the macro-crack. The initial state of the RVE used for the integration points on the crack surface is obtained by loading the RVE (with boundary conditions shown in figure 1) from the undeformed state to  $\alpha t_M^{loc}$ . The secant matrix  $\mathbf{D}$  can be calculated by unloading the deformed RVE at the converged state of the unloading step using equation (15). Taking  $\alpha=1.0$  shows divergence of the solution. Here  $\alpha = 0.99$  is used. More discussions on parameter  $\alpha$  and its effects on the results can be found in [4].

The failure zone averaging scheme is used to compute averaged quantities for the meso-scale model. It should be noted that in this scheme, the averaged quantities are calculated over the active damaged zone which contains integration points which are damaged and are loading. The active damage zone,  $\Omega_d$ , can be expressed mathematically as  $\Omega_d = \{x \in \Omega_m \mid \omega(x) > 0, f(x) = 0\}$ . The meso-scale quantities can be defined through:

$$l = \frac{|\Omega_m|}{h}, \quad \langle \varepsilon_m \rangle_{dam} = \frac{1}{|\Omega_d|} \int_{\Omega_d} \varepsilon_m d\Omega, \\ \mathbf{u}_{dam} = \langle \varepsilon_m \rangle_{dam} \cdot (l\mathbf{n}) \quad (20)$$

where  $|\cdot|$  represents the area of the domain.  $h$  and  $\mathbf{n}$  are the height of the RVE and normal to the crack band, respectively.  $l$  is the width of the localization band.  $\mathbf{u}_{dam}^0$  is calculated at the moment of crack initiation using above equations. By solving the system of equations (11) and (18), one can find the macroscopic traction,  $t_M$ , and cohesive tangent,  $\mathbf{T}_M$ . More details on theoretical and computational aspects can be found in [3, 4].

### 3 CRACKING CRITERIA

In the discontinuous computational homogenization scheme, the maximum principle macroscopic stress is used to determine the initiation and the direction of the crack. However, in the continuous-discontinuous scheme, loss of hyperbolicity criterion is employed for crack initiation and propagation. The hyperbol-

icity indicator is defined as [14]:

$$e = \min_{\mathbf{n}, \mathbf{h}} (n_i h_j A_{ijkl} n_k h_l) \quad (21)$$

where  $\mathbf{n} = (\cos \theta, \sin \theta)$  shows the normal vector to the crack surface and  $\mathbf{h}$  is assumed to be parallel to  $\mathbf{n}$ . Tensor  $\mathbf{A}$  is defined as:

$$A_{ijkl} = D_{ijkl} + \sigma_{ij} \delta_{kl} \quad (22)$$

in which  $\mathbf{D}$  is the tangent modulus. Based on this criterion the momentum equation loses hyperbolicity when  $e < 0$  and vector  $\mathbf{n}$  that minimizes  $e$  is normal to the direction of the crack (localization). In the multi-scale analysis, this criterion can be used to detect localization in the RVE. At each time step, from the homogenized tangent modulus,  $\mathbf{D}_M$ , tensor  $\mathbf{A}$  can be calculated using equation (22). Initiation and direction of the localization can then be determined using equation (21). The advantage of this criterion is that both initiation and direction of the crack can be obtained from the local-scale model.

### 4 RATE-DEPENDENT COHESIVE LAW

Two sources of rate dependency in concrete materials [15] are (1) viscoelasticity in the bulk material, and (2) the rate process of the bonds breakage in the fracture process zone. At high strain rate dynamic loading, the latter is the dominant mechanism which causes the cohesive law to be rate dependent. Bažant [15, 16], by considering fracture as a thermally activated phenomenon, derived a rate-dependent softening law. Here, we consider mode I fracture and for the traction in normal direction to the crack surface, the rate dependent softening law can be written as:

$$t_M^x \left( \llbracket u \rrbracket_M^x, \llbracket \dot{u} \rrbracket_M^x \right) = \left[ 1 + c_1 \operatorname{asinh} \left( \frac{\llbracket \dot{u} \rrbracket_M^x}{c_0} \right) \right] t_M^{0x} \quad (23)$$

where  $\llbracket \dot{u} \rrbracket_M^x$  denotes the macro crack opening rate and  $t_M^{0x}$  is the traction under static loading condition.  $c_0$  and  $c_1$  are material parameters.

Here, we assume that, when a crack initiates, the damage threshold,  $\kappa_I$ , in the gradient damage model which is used for meso-scale model,

is dependent on the crack opening rate through:

$$\kappa_I \left( \left[ \dot{u} \right]_M^x \right) = \left[ 1 + c_1 \operatorname{asinh} \left( \frac{\left[ \dot{u} \right]_M^x}{c_0} \right) \right] \kappa_I^0 \quad (24)$$

in which  $\kappa_I^0$  is the static damage threshold. In order to investigate this assumption, cohesive laws are computed for various values of  $\kappa_I$  which are obtained from equation (24) for  $\left[ \dot{u} \right]_M^x = 0.0, 0.25, 0.5, 1.0$  (m/s). Here,  $c_0$  and  $c_1$  are taken equal to 0.8 and 0.5, respectively. In figure 3, these results are shown with solid lines. The dashed lines depict the static cohesive law,  $t_M^{0x}$ , multiplied by  $\frac{\kappa_I \left( \left[ \dot{u} \right]_M^x \right)}{\kappa_I^0}$ . From figure 3, it can be concluded that:

$$t_M^x \left( \left[ u \right]_M^x, \left[ \dot{u} \right]_M^x \right) \simeq \frac{\kappa_I \left( \left[ \dot{u} \right]_M^x \right)}{\kappa_I^0} t_M^{0x} \quad (25)$$

The above relation shows that equations (23) and (24) are almost equivalent. So, in order to capture rate dependency effects in the macro-scale cohesive law, one can insert rate effects in the meso-scale model using equation (24).

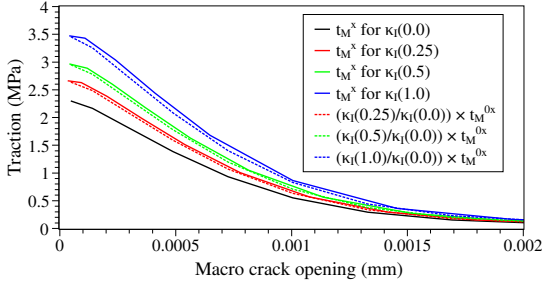


**Figure 3:** Traction-macro crack opening for various  $\kappa_I$ .

## 5 RESULTS AND DISCUSSION

In this section two examples will be discussed. First, a problem with a simple voided structure presented with which the multi-scale model is verified by comparison with a DNS model. In the voided structure case, the discontinuous homogenization scheme is used. In the second example, a complex random meso structure is used for the heterogeneous structure of

concrete. In the second case, both discontinuous and continuous-discontinuous schemes are used and the results are compared.

### 5.1 Multi-scale wave propagation problem in a beam with voided structure

Figure 4 shows a heterogeneous beam which is subjected to a constant velocity at both ends. Tensile waves propagate through the beam and after superposition of the waves at the center of the beam, the stress at this point exceeds the tensile strength and a crack initiates. Figure 5 shows the multi-scale model of the problem. Voided structures with different sizes are chosen as RVE for this problem. It should be mentioned that the multi-scale scheme is applied only on the crack and the bulk part is solved using the standard finite element method. The material properties for the RVE and the bulk material are given in table 1. A constant velocity equal to 0.3 (m/s) is applied at both ends of the beam. Cohesive laws computed from different RVE sizes, according to the failure zone averaging scheme, are illustrated in figure 6. It can be observed that the results are objective with respect to RVE size. In order to verify the multi-scale model, the results are compared with a DNS model. Figure 7 depicts the DNS model in which the material properties of the voided part and bulk part are similar to those of the RVE and the bulk part of the multi-scale model. Averaged stress over active damage zone versus damage opening,  $u_{dam}$ , for the DNS model and the multi-scale model are shown in figure 8, which shows good agreement. The difference between the results in the elastic branch is due to the fact that the mesostructure is not present in the multi-scale model before crack initiation and we do not use averaged properties for the bulk part before crack presence.

Rate effects can be included in the model using equation (24). In the solution procedure, at time step  $t_i$ , for a certain crack in the macro-scale model, the crack opening rate is calculated and then the strain threshold for the RVE corresponding to the integration points on this crack is updated.

The problem described in figure 4 is now considered for a crack with a rate-dependent cohesive law. The multi-scale problem is solved for different loading rates. Figure 9 illustrates the computed cohesive laws for various RVE sizes at different loading rates. As it can be observed in this figure, for a given crack opening, the maximum traction increases with loading rate. It is also obvious that the obtained softening laws are objective with respect to the RVE size. Figure 10 depicts averaged stress over the active damage zone versus damage opening for DNS model and multi-scale model at various loading rates. As can be observed in this figure, the curves are on top of each other for static loading and loading rates 0.3 (m/s) and 0.45 (m/s). This certifies the assumption of neglecting inertia effects at the local-scale model. For loading rate 1.0 (m/s), however, the result obtained from the multi-scale model differs from that of the DNS model. This difference is due to the fact that in higher loading rates the inertia forces around voided parts in DNS model increase but in the multi-scale model, inertia forces are neglected for the RVE. However, at this loading rate, the multi-scale model is capable of properly calculating the material response. In order to show this fact, the density of the voided part in the DNS model is assumed to be artificially small so that the inertia forces around the damaged zone are negligible. Averaged stress-damage opening curves are shown for  $V_0=1.0$  (m/s) in figure 11. It can be observed that the curves for the DNS model and the multi-scale model lie on top of each other when the inertia forces are neglected in the voided part.

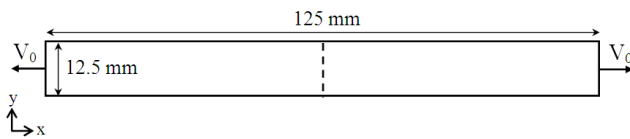


**Figure 4:** Beam under dynamic loading.

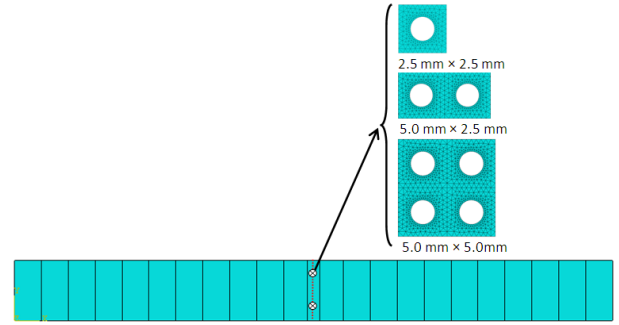


**Figure 5:** Multi-scale model and different RVE sizes.

**Table 1:** Material properties for bulk material and RVE.

		Bulk	RVE
$E$	[N/m <sup>2</sup> ]	50e9	50e9
$\nu$	[—]	0.2	0.2
$\kappa_I$	[—]	0.3	8e-5
$\alpha$	[—]	0.99	0.99
$\beta$	[—]	1500	1500
$\rho$	[kg/m <sup>3</sup> ]	1200	1200
$c$	[m <sup>2</sup> ]	4e-8	4e-8

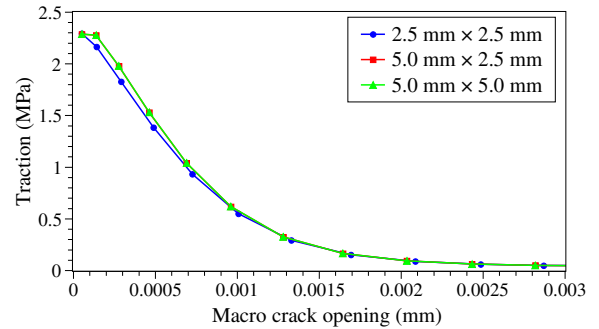


**Figure 6:** Computed cohesive law for different RVE sizes.

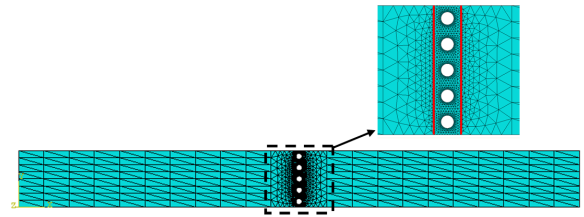


**Figure 7:** DNS model.

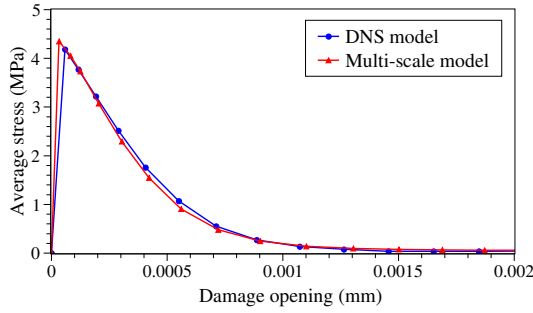


**Figure 8:** Comparison of averaged stress over failure zone vs. damage opening for multi-scale model and DNS model.

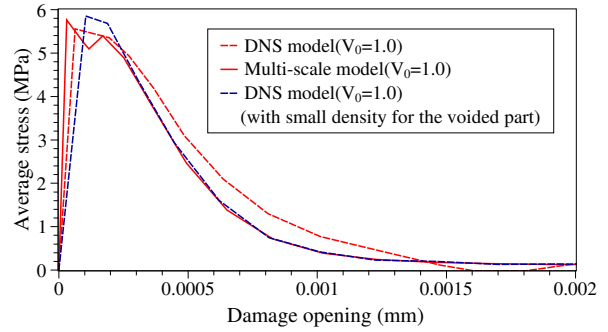


**Figure 11:** Inertia force effect on averaged stress-damage opening curve.

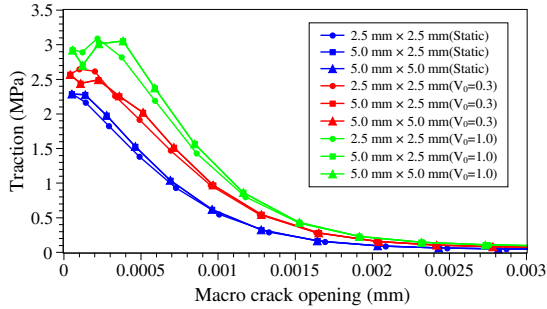


**Figure 9:** Computed cohesive laws for different RVE size at various loading rates.

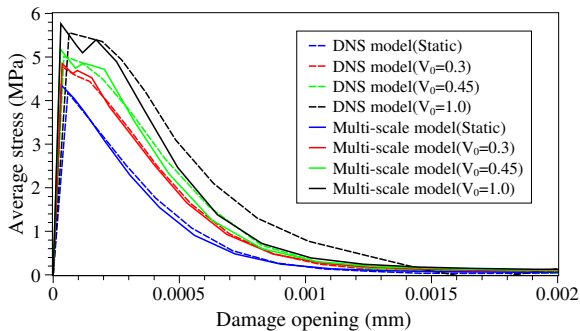


**Figure 10:** Averaged stress over the active damage zone versus damage opening for DNS model and multi-scale model.

## 5.2 Multi-scale wave propagation problem in a beam with random structure

In this section, a beam made of a heterogeneous three-phase material is considered. Both discontinuous and continuous-discontinuous schemes are used to compute rate dependent cohesive laws for cracking in this structure. The three phases include circular aggregates, an interfacial transition zone (ITZ) and matrix. The size of aggregates is in the range of 1.25 mm to 2.5 mm and they are randomly distributed in the matrix. The width of the ITZ is 0.25 mm and the aggregate density is 45%.

The multi-scale model is shown in figure 12. Loading and boundary conditions are the same as in the problem described in figure 4. The length and width of the beam are 800 mm and 125 mm, respectively. Material properties for the RVE are given in table 2. In order to reduce the computational time for this problem, multi-scale analysis is only applied to the middle element and all other elements are assumed to be elastic material with Young's modulus of  $30e9$  Pa and Poisson ratio of 0.2. The material constants  $c_0$  and  $c_1$  from equation (24) are 0.2 and 1.0, respectively. Three different sizes for the RVE with random structure are used.

Traction-separation curves for the different RVE sizes at various loading rates using the discontinuous homogenization scheme are shown in figure 13. It can be observed from figure 13 that the traction-separation curves are inde-

pendent of RVE size. Figure 14 demonstrates traction-separation curves using the continuous-discontinuous scheme. Objectivity of the results with respect to the RVE size can also be observed in this figure. To compare discontinuous and continuous-discontinuous schemes, the rate dependent cohesive laws for the case of RVE size  $20 \text{ mm} \times 20 \text{ mm}$  are shown in figure 15. For static loading, traction-separation curves obtained from the two schemes are on top of each other. However, for dynamic loading, the traction-separation curves obtained from the continuous-discontinuous scheme are smoother at smaller macro crack opening values and seem to be more precise. This can be explained from the fact that in the discontinuous computational homogenization scheme, the crack initiates in the model as soon as the maximum principle stress criterion is satisfied and it is not able to model damage prior to crack initiation (softening regime). As a result, there is no smooth transition between the linear regime and the softening regime solution. Figure 16 depicts the hyperbolicity indicator values for different RVE sizes using strain-rate independent and strain-rate dependent models at loading rate  $0.05 \text{ (m/s)}$  at crack initiation time. It can be observed that the rate dependency delays crack initiation. The angle associated to the minimum value of the hyperbolicity indicator shows the angle of normal vector to the macro crack surface. This angle for  $10 \text{ mm} \times 10 \text{ mm}$  RVE is  $-1.8^\circ$  and zero for  $15 \text{ mm} \times 15 \text{ mm}$  and  $20 \text{ mm} \times 20 \text{ mm}$  RVEs.

**Table 2:** Material properties for RVE.

		Matrix	Aggregate	ITZ
$E$	$[\text{N/m}^2]$	$25\text{e}9$	$30\text{e}9$	$20\text{e}9$
$\nu$	$[-]$	$0.2$	$0.2$	$0.2$
$\kappa_I$	$[-]$	$7\text{e-}6$	$0.3$	$3\text{e-}6$
$\alpha$	$[-]$	$0.99$	$0.99$	$0.99$
$\beta$	$[-]$	$1500$	$1500$	$1500$
$\rho$	$[\text{kg/m}^3]$	$1200$	$1200$	$1200$
$c$	$[\text{m}^2]$	$2\text{e-}7$	$2\text{e-}7$	$2\text{e-}7$

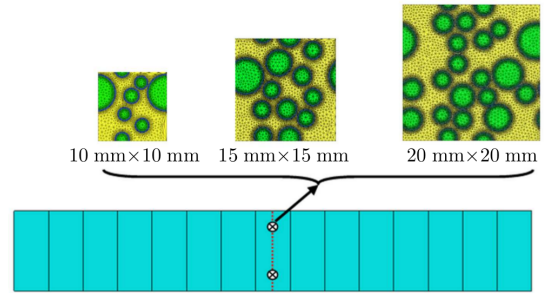


**Figure 12:** Multi-scale model.

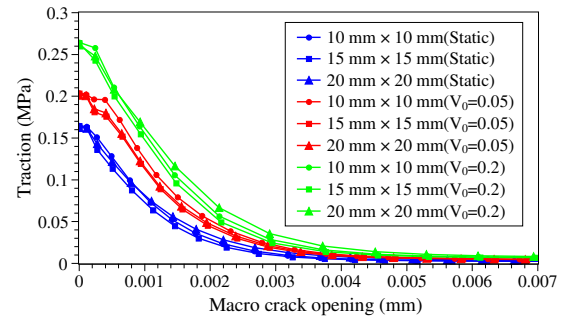


**Figure 13:** Cohesive law for various RVE size using discontinuous computational homogenization scheme.

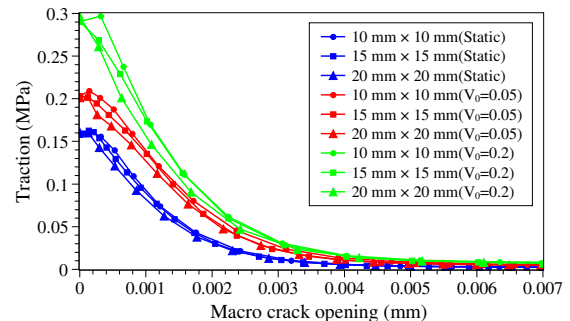


**Figure 14:** Cohesive law for various RVE size using continuous-discontinuous computational homogenization scheme.

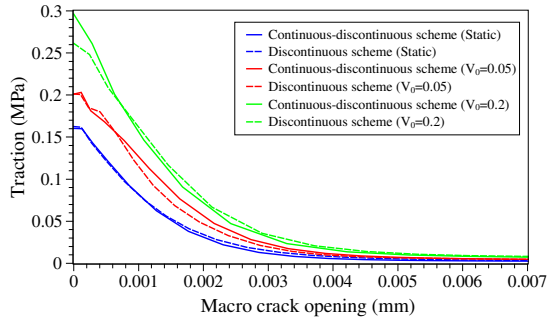


**Figure 15:** Comparison of the traction-separation curves for discontinuous and continuous-discontinuous schemes at different loading rates using a 20 mm  $\times$  20 mm RVE.

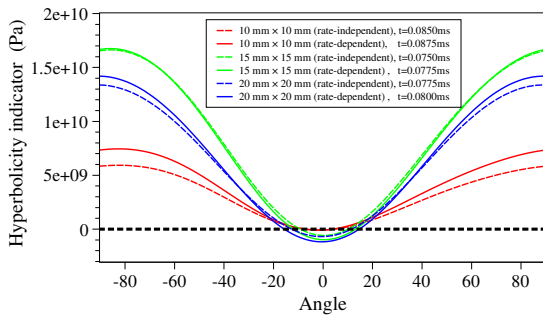


**Figure 16:** The hyperbolicity indicator for different RVE sizes using rate-independent and rate-dependent models at loading rate 0.05 (m/s).

## 6 CONCLUSIONS

A rate-dependent multi-scale crack model for heterogeneous materials under dynamic loading is presented. Both discontinuous and continuous-discontinuous computational homogenization schemes are used to obtain rate-dependent cohesive laws for the crack. Verification studies are performed by comparing the results from the multi-scale model and the DNS model which show a good agreement. It can also be concluded that in case of a large macroscopic wave length compared to RVE size, one can neglect the inertia effects at the local-scale model. Objectivity of the results with respect to RVE size are shown for both discontinuous and continuous-discontinuous schemes. The comparison between the traction-separation curves obtained from continuous-discontinuous and

continuous schemes shows that the continuous-discontinuous scheme gives better results. The hyperbolicity indicator which is calculated using the homogenized tangent modulus is used to detect initiation and direction of the crack in the continuous-discontinuous scheme. The results show that a correct direction can be calculated with this criterion. This study can be extended to more complicated dynamic crack propagation problems.

## REFERENCES

- [1] Gitman, I., Askes, H. and Sluys, L.J., 2007. Representative volume: existence and size determination. *Engrg. Fract. Mech.* **74(16)**:2518–2534.
- [2] Nguyen, V. P., Lloberas-Valls, O., Stroeven, M. and Sluys, L.J., 2011. Homogenization-based multiscale crack modelling: From microdiffusive damage to macro-cracks. *Comput. Methods Appl. Mech.* **200**:1220–1236.
- [3] Nguyen, V. P., Lloberas-Valls, O., Stroeven, M. and Sluys, L.J., 2010. On the existence of representative volumes for softening quasi-brittle materials—a failure zone averaging scheme. *Comput. Methods Appl. Mech. Engrg.* **199**:3028–3038.
- [4] Nguyen, V. P., Stroeven, M. and Sluys, L.J., 2012. An enhanced continuous-discontinuous multiscale method for modeling mode-I cohesive failure in random heterogeneous quasi-brittle materials. *Engrg. Fract. Mech.* **79**:78–102.
- [5] Fish, J. and Chen, W., 2001. Higher-order homogenization of initial/boundary value problem. *J. Eng. Mech.* **127(12)**:1223–1230.
- [6] Chen, W. and Fish, J., 2001. A dispersive model for wave propagation in periodic heterogeneous media based on homogenization with multiple spatial and temporal scales. *J. Appl. Mech.* **68**:153–161.

- [7] Souza, F. V., Allen, D. H. and Kim, M. R., 2008. Multiscale model for predicting damage evolution in composites due to impact loading. *Compos. Sci. Technol.* **68**:2624–2634.
- [8] Souza, F. V. and Allen, D. H., 2010. Multiscale modeling of impact on heterogeneous viscoelastic solids containing evolving microcracks. *Int. J. Numer. Meth. Engng.* **82**:464–504.
- [9] Moes, N., Dolbow, J. and Belytschko, T., 1999. A finite element method for crack growth without remeshing. *Int. J. Numer. Methods Engng.* **46**(1):131–150.
- [10] Peerlings, P., De Borst, R., Brekelmans, W. and De Vree, J., 1996. Gradient enhanced damage for quasi-brittle materials. *Int. J. Numer. Methods Engrg.* **39**:3391–3403.
- [11] Lemaitre, J., 1996. A Course on Damage Mechanics. *Springer-Verlag*.
- [12] Mazars, J. and Pijaudier-Cabot, G., 1989. Continuum damage theory-application to concrete. *J. Engng. Mech. Div. ASCE* **115**. 345–365.
- [13] Kouznetsova, V., Brekelmans, W.A.M., Baaijens, F.P.T., 2001. An approach to micro-macro modeling of heterogeneous materials. *Comput. Mech.* **27**(1):37–48.
- [14] Belytschko, T., Chen, H., Xu, J. and Zi, G., 2003. Dynamic crack propagation based on loss of hyperbolicity and a new discontinuous enrichment. *Int. J. Numer. Meth. Engng.* **58**:1873–1905.
- [15] Cusatis, G., 2011. Strain-rate effects on concrete behavior. *Int. J. Impact Eng.* **38**:162–170.
- [16] Bažant, Z., 1995. Creep and damage in concrete. *Materials science of concrete IV*. 355–389.